











TOI-1173 A *b*: The First Inflated Super-Neptune in a Wide Binary System

JHON YANA GALARZA ^{1,*}, THIAGO FERREIRA ², DIEGO LORENZO-OLIVEIRA ³, JOSHUA D. SIMON ¹,
HENRIQUE REGGIANI ⁴, ANTHONY L. PIRO ¹, ANDREW MCWILLIAM ¹, YURI NETTO ⁵, ADRIANA VALIO ⁵ AND
DAVID R. CIARDI ⁶

¹*The Observatories of the Carnegie Institution for Science, 813 Santa Barbara Street, Pasadena, CA 91101, USA*

²*Department of Astronomy, Yale University, 219 Prospect Street, New Haven, CT 06511, USA*

³*Laboratório Nacional de Astrofísica, Rua Estados Unidos 154, 37504-364, Itajubá - MG, Brazil*

⁴*Gemini South, Gemini Observatory, NSF's NOIRLab, Casilla 603, La Serena, Chile*

⁵*Center for Radio Astronomy and Astrophysics Mackenzie (CRAAM), Mackenzie Presbyterian University, Rua da Consolação, 896, São Paulo, Brazil*

⁶*NASA Exoplanet Science Institute, IPAC, California Institute of Technology, Pasadena, CA 91125 USA*

ABSTRACT

Among Neptunian mass planets exoplanets ($20\text{--}50\text{ M}_{\oplus}$), puffy hot Neptunes are extremely rare, and their unique combination of low mass and extended radii implies very low density ($\rho < 0.3\text{ g cm}^{-3}$). Over the last decade, only a few puffy planets have been detected and precisely characterized with both transit and radial velocity observations, most notably including WASP-107 *b*, TOI-1420 *b*, and WASP-193 *b*. In this paper, we report the discovery of TOI-1173 A *b*, a low-density ($\rho = 0.269^{+0.028}_{-0.024}\text{ g cm}^{-3}$) super-Neptune with $P = 7.06$ days in a nearly circular orbit around the primary G-dwarf star in the wide binary system TOI-1173 A/B. Using radial velocity observations with the MAROON-X spectrograph and transit photometry from TESS, we determined a planet mass of $M_p = 26.1 \pm 1.9\text{ M}_{\oplus}$ and radius of $R_p = 8.10 \pm 0.17\text{ R}_{\oplus}$. TOI-1173 A *b* is the first puffy Super-Neptune planet detected in a wide binary system (separation $\sim 11,400\text{ AU}$). We explored several mechanisms to understand the puffy nature of TOI-1173 A *b*, and showed that tidal heating is the most promising explanation. Furthermore, we demonstrate that TOI-1173 A *b* likely has maintained its orbital stability over time and may have undergone von-Zeipel-Lidov-Kozai migration followed by tidal circularization given its present-day architecture, with important implications for planet migration theory and induced engulfment into the host star. Further investigation of the atmosphere of TOI-1173 A *b* will shed light on the origin of close-in low-density Neptunian planets in field and binary systems, while spin-orbit analyses may elucidate the dynamical evolution of the system.

Keywords: Exoplanets (498), Hot Neptunes (754), Wide binary stars (1801), Radial velocity (1332), Transit photometry (1709), Exoplanet detection methods (489), Exoplanet astronomy (486), Transits (1711)

1. INTRODUCTION

The discovery of 51 Peg *b* (Mayor & Queloz 1995) revolutionized our understanding of planet formation and evolution due to the surprising result that gas giant planets could be observed relatively close to main-sequence stars. This finding hints not only that exoplanets are

formed through core accretion of gaseous protoplanetary disc material (Pollack et al. 1996), but that it is also possible that planets might originate at a wide distance from their host star and subsequently undergo migration (Rice & Armitage 2003; Ida & Lin 2004). In a similar aspect, despite exhibiting similar masses to the Solar System gas/ice giant planets, inflated radii planets present an enigma, boasting extended and diffuse atmospheres that defy conventional models for planet formation and evolution (e.g., Lee & Chiang 2015; Lopez & Fortney 2014a, and references therein). These planets constitute

Corresponding author: J. Yana Galarza
jyanagalarza@carnegiescience.edu

* Carnegie Fellow

a category characterized by an uncommon combination of large sizes and exceptionally low densities ($\rho \leq 0.3 \text{ g cm}^{-3}$), aptly named puffy¹ planets.

Their proximity to their host stars could be responsible for the heating and expansion of their atmospheres (Batygin & Stevenson 2010; Pu & Valencia 2017; Thorngren & Fortney 2018), which contributes to their observed low density. For objects with equilibrium temperatures exceeding 1000 K, the inflated radius mechanism may be similar to hot Jupiter planets (Fortney et al. 2021a), i.e., (a) due to thermal contraction of He/H atmospheres (Owen & Wu 2013; Lopez & Fortney 2014a), (b) atmospheric winds driven by photo-ionisation due to intense UV radiation from the host star (Murray-Clay et al. 2009), which can be probed by observing larger transit depths due to atmospheric expansion in the Lyman- α line at $\lambda = 1215.6 \text{ \AA}$ signatures in a planet’s spectrum (Kislyakova et al. 2019; Owen et al. 2023), H α absorption at $\lambda = 6562.8 \text{ \AA}$ (Jensen et al. 2012; Christie et al. 2013; Cauley et al. 2017), or the Helium triplet in the near-infrared at $\lambda = 10\,833 \text{ \AA}$ (Spake et al. 2018; dos Santos et al. 2020; Vissapragada et al. 2020; Orell-Miquel et al. 2022; Bennett et al. 2023; Krolkowski et al. 2024), and/or (c) photo-chemical hazes in the atmosphere responsible for larger and puffier appearance (Gao & Zhang 2020a; Ohno & Tanaka 2021). Nevertheless, these mechanisms may not fully elucidate the large radii observed in the lowest density planets with equilibrium temperatures below 1000 K, which poses an additional challenge in incorporating such phenomena into existing exoplanet formation models.

Puffy planets are extremely rare, with only 5 planets in the intermediate-mass regime ($20M_{\oplus} \leq M_p \leq 50M_{\oplus}$) with densities below $\rho \leq 0.3 \text{ g cm}^{-3}$ (per The Extrasolar Planets Encyclopædia² as of March 2024) in single stars, and none detected in binary systems. These exoplanets are HATS-8 *b* (Bayliss et al. 2015), TOI-1420 *b* (Yoshida et al. 2023), TOI-2525 *b* (Trifonov et al. 2023), WASP-107 *b* (Anderson et al. 2017), and WASP-193 *b* (Barkaoui et al. 2023), which were detected by both the radial velocity and transit methods. Planets in this category are intrinsically important in deciphering the mechanisms that lead to runaway gaseous accretion despite their smaller cores, a phenomenon crucial to our understanding of planetary formation and evolution (Lissauer & Stewart 1993; Bitsch et al. 2015). It is noteworthy that only two objects in this sample (TOI-2525 *b* and

WASP-107 *b*) belong to multi-planet systems, and all orbit stars with effective temperatures above 4400 K.

This paper presents the discovery of a low-density inflated super-Neptune ($M_p = 26.1 M_{\oplus}$) found in orbit around an 8.7 Gyr old G-dwarf star, completing each orbit in ~ 7.068 days. The TOI-1173 system contains two stars, the planet-hosting component TOI-1173 A, and TOI-1173 B, which lacks any detected exoplanets (Yana Galarza et al. 2024, submitted). This system is the second wide binary with a separation greater than 10,000 AU discovered to host planets after HAT-P-4 A (29,500 AU; Mugrauer et al. 2014).

In Section 2 we describe the spectroscopic and photometric observations of TOI-1173 A with MAROON-X and TESS, respectively. In Section 3, we present a Keplerian model, and in Section 4, we discuss the origin of the close-in low-density nature of TOI-1173 A *b* plus the relevant timescales for the dynamical evolution of this TOI-1173 A/B system. Lastly, we provide an overview of our findings and discuss future research prospects in Section 5.

2. OBSERVATIONS

2.1. TESS Photometry

TOI-1173 A (TIC 232967440) was observed by the Transiting Exoplanet Survey Satellite (TESS; Ricker et al. 2015) during Sectors 14, 15, 21, 22, 41, 47, and 48. TESS light curves of TOI-1173 A³ revealed several periodic transits, leading to the detection and announcement of TOI-1173 A *b* (TOI-1173.01⁴) as a transiting planet candidate by the TESS Science Office (TSO) (Guerrero et al. 2021). We retrieved the two-minute cadence observations, which were processed by the Science Processing Operations Centre (SPOC; Jenkins et al. 2016) standard aperture pipeline, using the LIGHTKURVE⁵ software (Lightkurve Collaboration et al. 2018). Outliers in the data were removed with an upper median sigma-clipping of 2, and afterwards, we retrieved a prominent modulation period of 7.068 days ($t_0 = 2423.4$ at BTJD-2457000 days) using a Box-Fitting Least Squares Algorithm (BLS⁶; Kovács et al. 2002; Bhatti et al. 2021) in a period grid spanning from 0.25 to 100 days (see upper panel in Figure 1).

To remove systematic instrumental trends characterized by a gradual increase/decrease in the apparent stel-

¹ Super-puff planets are worlds with sub-Neptune masses ($\leq 5M_{\oplus}$) but with radii comparable to gas-giants ($\geq 4R_{\oplus}$), leading to extremely low densities ($\leq 0.1 \text{ g cm}^{-3}$).

² <https://exoplanet.eu/home/>

³ All the TESS data used in this paper can be found in MAST: [10.17909/dpx3-gv19](https://exoplanet.eu/home/)

⁴ https://exo.mast.stsci.edu/exomast_planet.html?planet=TOI1173.01

⁵ <https://docs.lightkurve.org/>

⁶ <https://astrobase.readthedocs.io/>

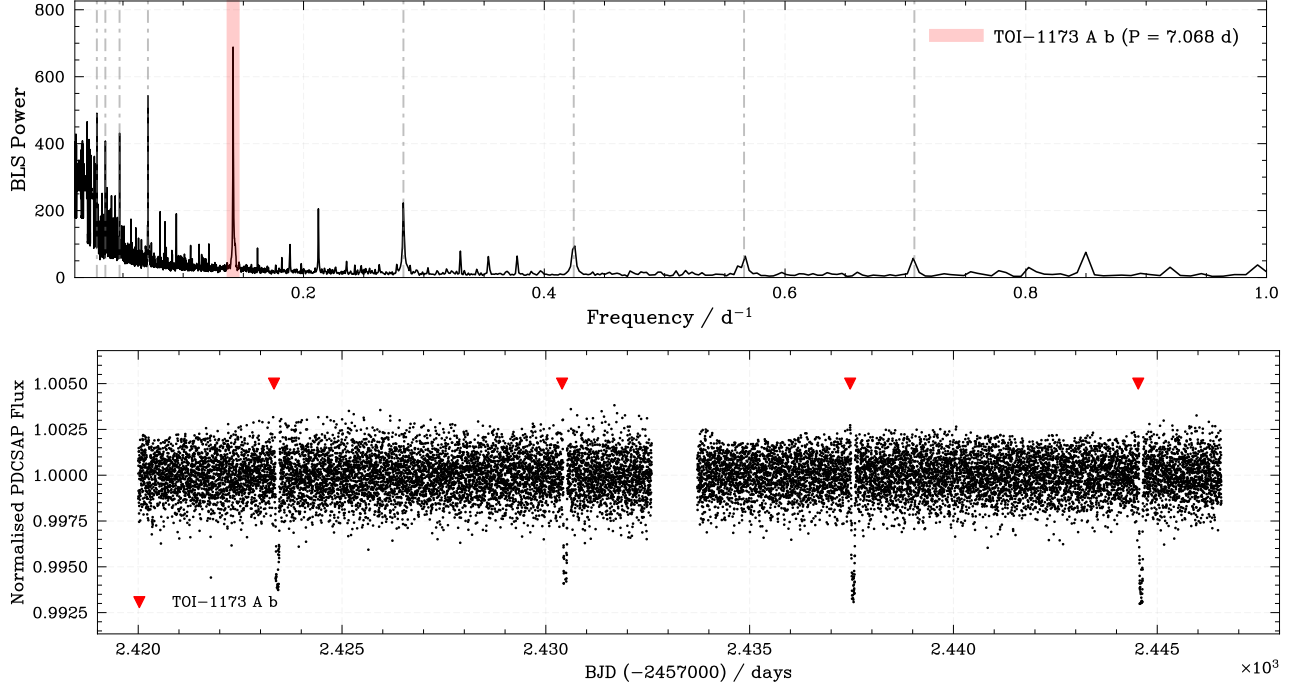


Figure 1. *Upper panel:* BLS periodogram for TOI-1173 A *b*'s observations. The prominent period of $P = 7.068$ days is indicated as a red strip, along with lower (P/n , $n = 1, 2, 3, 4$) and upper ($P \times n$) harmonics in gray. *Bottom panel:* Detrended TESS two-minute cadence light curve of one sector. Red triangles indicate the TOI-1173 A *b* transits visible every 7.068 days.

Table 1. Priors for TOI-1173 A's TESS GP de-trending model. $\mathcal{LU}(\alpha, \beta)$ stands for a log-Uniform distribution between α and β , and $\mathcal{N}(\mu, \sigma)$ stands for a Normal distribution with mean μ and standard deviation σ .

Parameter	Value	Prior
Offset; $\mathcal{M}_{\text{GP}} \times 10^{-4}$	$0.86^{+2.43}_{-2.29}$	$\mathcal{N}(0, 0.1)$
Jitter; σ_W	$1.69^{+153.02}_{-1.69}$	$\mathcal{LU}(10^{-6}, 10^6)$
Amplitude; $\sigma_{\text{GP}} \times 10^{-4}$	$7.23^{+1.60}_{-1.08}$	$\mathcal{LU}(10^{-6}, 10^6)$
GP Timescale; ρ_{GP}	$1.22^{+0.26}_{-0.17}$	$\mathcal{LU}(0.001, 1000)$

lar flux over time, we applied a de-trending model to the light curve using the JULIET⁷ software (Espinoza et al. 2019), based on Gaussian Process (GP) regression. With this approach, two observations t_i and t_j are related via the kernel

$$k(\tau_{i,j}, \sigma) = \sigma_{\text{GP}}^2 \cdot \mathfrak{M}(\tau_{i,j}, \rho) + (\sigma_i^2 + \sigma_W^2) \delta_{i,j}, \quad (1)$$

where $k(\tau_{i,j})$ is the i, j -th element of the covariance matrix Σ , $\tau_{i,j}$ is the absolute difference between the two subsequent observations, σ_i is the uncertainty of

the i -th element (fluxes), σ_{GP} is the amplitude of the process, σ_W is a jitter term, $\delta_{i,j}$ is a Kronecker delta function, and $\mathfrak{M}(\tau_{i,j}, \rho)$ is the Matérn segment of the kernel with characteristic length-scale ρ (Rasmussen & Williams 2006).

The Markov hyper-parameter space for the de-trending model was probed using a dynamic nested sampling method (DYNESTY⁸; Speagle 2020) over 1500 walkers in 1000 steps, with the first half of the chains burned-in. The hyper-priors are listed in Table 1 and the detrended light curve of one sector is depicted at the bottom of Figure 1.

2.2. MAROON-X Radial Velocity

To confirm the planetary nature of the transit signal, we obtained 10 epochs of spectroscopy of TOI-1173 A with the high-resolution echelle spectrograph MAROON-X (Seifahrt et al. 2018, 2022) mounted on the 8.1 m Gemini North Telescope of The International Gemini Observatory located in Hawaii (programme ID GN-2022A-Q-227; PI: Yuri Netto). The MAROON-X data were reduced using a custom Python 3 data reduction, which is incorporated into Gemini's DRAGON platform. The radial velocities are provided in Table 2.

⁷ <https://juliet.readthedocs.io/en/latest/>

⁸ <https://dynesty.readthedocs.io/en/stable/>

Table 2. Radial velocities for TOI-1173 A collected with the MAROON-X/Gemini spectrograph. The reference radial velocity is $V_{\text{ref.}} = -45.66 \text{ km s}^{-1}$.

Time (BJD)	$\Delta RV \text{ (m s}^{-1}\text{)}$	$\sigma_{RV} \text{ (m s}^{-1}\text{)}$	Channel
2459677.9802383	-6.242	1.574	Blue
2459678.9563171	-11.743	1.539	Blue
2459680.8670781	-6.320	1.572	Blue
2459682.9317091	8.074	1.176	Blue
2459688.9707073	1.052	1.409	Blue
2459690.0054999	5.499	1.024	Blue
2459696.8967542	6.519	1.029	Blue
2459780.7797433	0.617	0.996	Blue
2459791.7447053	-10.061	1.673	Blue
2459792.7445192	-12.011	1.265	Blue
2459677.9802383	-10.019	2.66	Red
2459678.9563171	-13.254	2.604	Red
2459680.8670781	-3.225	2.636	Red
2459682.9317091	7.355	2.038	Red
2459688.9707073	1.352	2.386	Red
2459690.0054999	4.750	1.802	Red
2459696.8967542	4.092	1.801	Red
2459780.7797433	3.972	1.828	Red
2459791.7447053	-5.789	2.997	Red
2459792.7445192	-9.456	2.247	Red

We employed the Generalised Lomb-Scargle method (GLS; [Zechmeister & Kürster 2009](#)) on a grid ranging from 0.1 to 200 days and detected a highly significant periodic signal at $P_{\text{LS}} = 7.076$ days; which is in line with the period found in the TESS data with a relative difference of $\Delta P = 0.008$ days. A Bayesian Information Criterion test (BIC; [Ivezić et al. 2014](#)) revealed a discrepancy of $\Delta \text{BIC} \approx 400$ between a periodic model and a non-varying model.

Stellar activity may sometimes simply add noise to the data, but in the worst scenario, it can mimic or masquerade as planetary signals. Therefore, we analysed five stellar activity proxies for TOI-1173 A using the SpEctrum Radial Velocity AnaLyser SERVAl pipeline⁹ ([Zechmeister et al. 2018](#)): the differential line width (dLW), chromatic index (CrX) and $H\alpha$ ($\lambda = 656.46 \text{ nm}$), and the Na D doublet ($\lambda = 589.0 \text{ nm}$ and 589.6 nm) for the Blue channel, as well as the Ca II IRT1, IRT2 and IRT3 infrared triplet ($\lambda = 849.8, 854.2, \text{ and } 866.2 \text{ nm}$) for the Red channel of the MAROON-X spectra.

At the companion’s orbital period, we did not observe any indication of significant timing or phase modula-

Table 3. Fundamental parameters of TOI-1173 A.

Parameter	TOI-1173 A	Units
Effective temperature (T_{eff})	5350 ± 34	K
Surface gravity ($\log g$)	4.450 ± 0.020	dex
Metallicity ($[\text{Fe}/\text{H}]$)	0.139 ± 0.065	dex
Microturbulence (v_t)	1.11 ± 0.01	km s^{-1}
Age (Γ)	$8.7^{+2.0}_{-1.9}$	Gyr
Mass (M_*)	$0.911^{+0.028}_{-0.030}$	M_{\odot}
Radius (R_*)	$0.934^{+0.011}_{-0.011}$	R_{\odot}
$v \sin i$	< 1.5	km s^{-1}

tions, which could commonly arise if the period were due to stellar activity cycles, such as atmospheric expansions or pulsations (e.g., [Sobolev 1960](#); [Doazan & Peton 1970](#)). Furthermore, we did not detect statistically meaningful correlations between these magnetic activity indicators and the radial velocity measurements, as evaluated by the Pearson– r correlation index and the null-hypothesis significance testing p -value (see Figure 2). This analysis strengthens the evidence in favour of a companion nature for the observed radial velocity variations at the retrieved prominent modulation period, and even in the presence of any significant stellar magnetic activity, we do not expect suppression of the companion’s signal.

Taking advantage of the high spectral resolution ($R = \lambda/\Delta\lambda = 85,000$) and signal-to-noise ratio ($\text{SNR} \sim 300$) of the coadded MAROON-X spectrum, we determined the fundamental parameters, meaning effective temperature, surface gravity, metallicity, mass, radius, and age of TOI-1173 A. The methodology is thoroughly explained in our companion paper (Yana Galarza et al., 2024, submitted). The results are listed in Table 3. TOI-1173 A is an old, slightly metal-rich late G star.

2.3. High-resolution Imaging

As part of our standard process for validating transiting exoplanets to assess the possible contamination of bound or unbound companions on the derived planetary radii ([Ciardi et al. 2015](#)), we observed TOI-1173 A with high-resolution near-infrared adaptive optics (AO) imaging at Keck Observatory.

The observations were made with the NIRC2 instrument on Keck-II behind the natural guide star AO system ([Wizinowich et al. 2000](#)) on 2020-May-28 UT in the standard 3-point dither pattern that is used with NIRC2 to avoid the left lower quadrant of the detector which is typically noisier than the other three quadrants. The dither pattern step size was $3''$ and was repeated twice, with each dither offset from the previous dither by $0.5''$. NIRC2 was used in the narrow-angle mode with a full

⁹ <https://github.com/mzechmeister/serval>

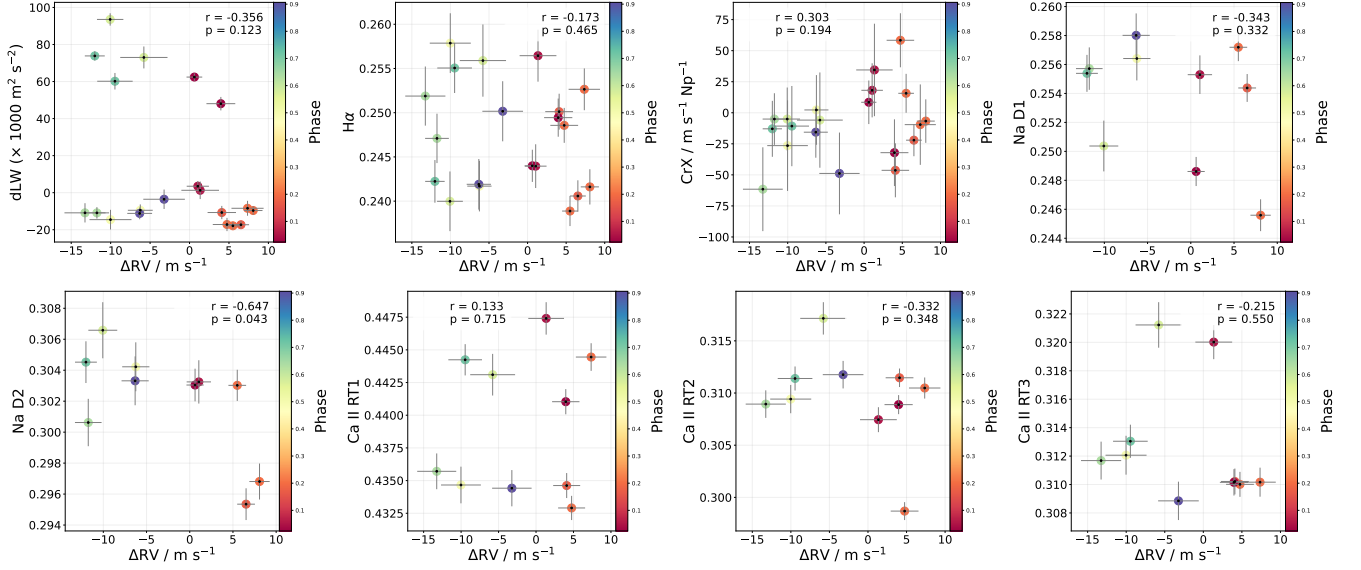


Figure 2. Radial velocity and the relationship with TOI-1173 A’s activity indicators dLW, CrX, H α , plus Na doublet for the Blue channel, and Ca II infrared triplet for the Red channel of MAROON-X spectra. Colors indicate the phase at $P_{LS} = 7.076$ days. The Pearson- r correlation index and the associated p -values are indicated at the top of each panel.

field of view of $\sim 10''$ and a pixel scale of approximately $0.0099442''$ per pixel. The Keck observations were made in the Br- γ filter ($\lambda_o = 2.1686$; $\Delta\lambda = 0.0326 \mu\text{m}$) with an integration time in each filter of 3 seconds for a total of 27 seconds.

Flat fields were generated from a median average of dark subtracted dome flats. Sky frames were generated from the median average of the 9 dithered science frames; each science image was then sky-subtracted and flat-fielded. The reduced science frames were combined into a single combined image using an intra-pixel interpolation that conserves flux, shifts the individual dithered frames by the appropriate fractional pixels; the final resolution of the combined dithers was determined from the full-width half-maximum of the point spread function; $0.0494''$. To within the limits of the AO observations, no stellar companions were detected. The final 5σ limit at each separation was determined from the average of all the determined limits at that separation and the uncertainty on the limit was set by the rms dispersion of the azimuthal slices at a given radial distance (see Fig. 3).

Furthermore, we also found independent analyses in the ExoFOP database based on ground-based time series of TOI-1173 A. These results confirm that the transit is caused by an exoplanet, a conclusion supported by our estimated transit and radial velocity periods.

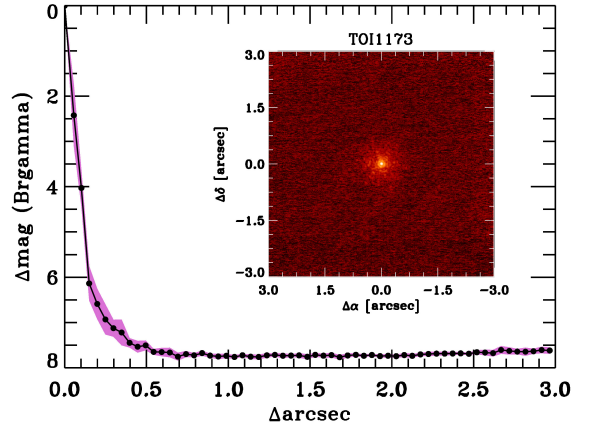


Figure 3. Companion sensitivity for the near-infrared adaptive optics imaging. The black points represent the 5σ limits and are separated in steps of 1 FWHM. The purple represents the azimuthal dispersion (1σ) of the contrast determinations (see text). The inset image is of the primary target showing no additional close-in companions.

We employed the ALLESFITTER¹⁰ software (Günther & Daylan 2021) for a joint transit and radial velocity Keplerian fit of TOI-1173 A b with free parameters including the orbital period (P), time of inferior conjunction (T_0), Doppler-induced RV semi-amplitude (K), the cosine of the orbital inclination ($\cos i$), the sum of stellar and companion radii divided by the semi-major axis

3. KEPLERIAN FIT

¹⁰ <https://www.allesfitter.com/>

$((R_p + R_\star)/a)$, limb-darkening coefficients q_1 and q_2 (see Kipping 2013 and Espinoza & Jordán 2016 for details), plus jitter terms for TESS and both MAROON-X channels. Considering also the possibility of another orbiting companion to TOI-1173 A, or that the modulations were in part due to stellar activity, we set uniform priors for the model barycentre motion $\dot{\gamma}$ and radial velocity intercept γ . These parameters are incorporated into the model in the form $\gamma + \dot{\gamma} \cdot (T - T_0)$, where T represent the time of the observations. Furthermore, we set the orbital eccentricity plus periastron argument coupled as Laplace parameters $\sqrt{e} \cos(\omega)$ and $\sqrt{e} \sin(\omega)$ to avoid Lucy-Sweeney degeneracy (Lucy & Sweeney 1971).

The Markov hyper-parameter space in this Keplerian model was also probed using DYNesty over 500 live points and tolerance of the convergence criterion of 0.01 (see details in Günther & Daylan 2021). The resulting parameters indicate a planet with mass $26.1 \pm 1.9 M_\oplus$ and radius $8.10 \pm 0.17 R_\oplus$ in a nearly circular ($e = 0.032$) orbit around TOI-1173 A every 7.06387 days (see Table 4 for the full Keplerian parameters). Figure 4 presents the best-fit 1-companion joint model for TOI-1173 A *b*.

4. DISCUSSION

4.1. TOI-1173 A *b*: A Low-density Super Neptune

In Figure 5, we present the discovery of TOI-1173 A *b* in context on a mass-radius diagram of other super-Neptune planets ($20M_\oplus \leq M_p \leq 50M_\oplus$) from the Encyclopædia of Exoplanetary System as of March 2024. The near neighbours to TOI-1173 A *b* are TOI-2525 *b* (Trifonov et al. 2023), WASP-107 *b* (Piaulet et al. 2021) and TOI-1420 *b* (Yoshida et al. 2023). The latter two are important targets for studies of planetary atmospheres. Both exoplanets share similar periods, masses, eccentricities and semi-major axes with TOI-1173 A *b*, but have larger radii, which leaves TOI-1173 A *b* somewhat denser than WASP-107 *b* and TOI-1420 *b*. Nonetheless, this comparison is relative to single stars. TOI-2525 *b* is an inflated exoplanet orbiting a K-dwarf star. However, it differs from TOI-1173 A *b* in its longer period (23 days), higher eccentricity (0.17), and larger semi-major axis (0.15 au). HATS-8 *b* (Bayliss et al. 2015) and WASP-193 *b* (Barkaoui et al. 2023) are also puffy Super-Neptune exoplanets; however, their equilibrium temperatures exceed 1000 K. Remarkably, WASP-193 *b* has the lowest density among all Super-Neptunes. This restricted sample of puffy Super-Neptunes with precisely measured masses and radii makes TOI-1173 A *b* a valuable addition to this population.

Additionally, TOI-1173 A *b* seems to follow the Cold-Hydrogen Equation-Of-State (EOS) of Becker et al. (2014) in the mass-radius relation. However, determin-

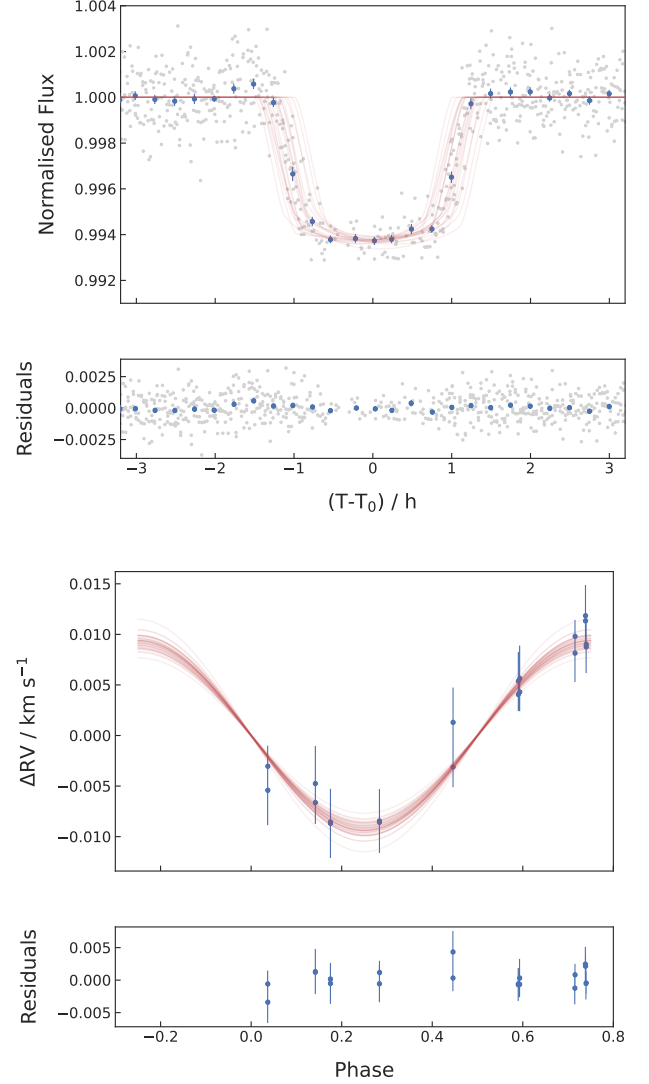


Figure 4. Phase-folded TESS light curve (upper panel) and MAROON-X radial velocity (bottom panel) joint models of TOI-1173A *b*. Red curves show 20 samples drawn from the posterior. The associated residuals are shown below each panel.

ing its composition and internal structure presents a challenge due to its inflated radius, which can create the impression that the planet shares a similar composition to Saturn and Jupiter.

Figure 6 is limited to the giant planets in the range of $0.01\text{--}10 M_{\text{Jup}}$ and $0.1\text{--}1.33 R_{\text{Jup}}$. From this figure, we observe that TOI-1173 A *b*, along with other Super-Neptunes, lies in a transition region. On one side are the low-mass, non-degenerate planets, where the bulk density decreases with increasing mass. On the other side are the high-mass, partially degenerate gas giants, where the bulk density increases with increasing mass.

Table 4. Orbital and physical parameters derived for TOI-1173 A *b*.
Note: $\mathcal{U}(\alpha, \beta)$ stands for a Uniform distribution between α and β .

	Parameter	Values	Prior
Model Fitted Planetary Parameters			
Orbital period (d)	P_b	$7.06387^{+0.00033}_{-0.00026}$	$\mathcal{U}(7.0524, 7.0724)$
Time of inferior conjunction (d - 2460000)	$T_{0;b}$	$392.9254^{+0.0080}_{-0.0064}$	$\mathcal{U}(392.660, 393.200)$
Doppler-induced RV semi-amplitude (m s^{-1})	K_b	$9.29^{+0.58}_{-0.53}$	$\mathcal{U}(0, 20)$
1st Laplace parameter	$\sqrt{e_b} \cos \omega_b$	0.03 ± 0.14	$\mathcal{U}(-1, 1)$
2nd Laplace parameter	$\sqrt{e_b} \sin \omega_b$	$-0.00^{+0.19}_{-0.13}$	$\mathcal{U}(-1, 1)$
Planet-to-star radius ratio	R_b/R_\star	0.0795 ± 0.0014	$\mathcal{U}(0, 1)$
Radii sum divided by semi-major axis	$(R_\star + R_b)/a_b$	$0.06676^{+0.00083}_{-0.00077}$	$\mathcal{U}(0, 1)$
Cosine of the Orbital Inclination	$\cos i_b$	$0.0472^{+0.0013}_{-0.0013}$	$\mathcal{U}(0, 1)$
TESS jitter (ppm)	$\ln \sigma_{\text{TESS}}$	-6.785 ± 0.020	$\mathcal{U}(-15, 0)$
MAROON-X Blue channel jitter (km s^{-1})	$\ln \sigma_{\text{jit.};\text{Blue}}$	$-7.04^{+0.49}_{-0.54}$	$\mathcal{U}(-15, 0)$
MAROON-X Red channel jitter (km s^{-1})	$\ln \sigma_{\text{jit.};\text{Red}}$	$-6.74^{+0.63}_{-0.67}$	$\mathcal{U}(-15, 0)$
MAROON-X Blue barycentre motion ($\text{km s}^{-1} \text{ d}^{-1}$)	$\gamma_{1;\text{Blue}}$	-0.00308 ± 0.00073	$\mathcal{U}(-1000, 1000)$
MAROON-X Red barycentre motion ($\text{km s}^{-1} \text{ d}^{-1}$)	$\gamma_{1;\text{Red}}$	$-0.0043^{+0.0011}_{-0.0012}$	$\mathcal{U}(-1000, 1000)$
MAROON-X Blue RV slope ($\text{km s}^{-1} \text{ d}^{-2}$)	$\dot{\gamma}_{1;\text{Blue}}$	-0.000003 ± 0.000012	$\mathcal{U}(-100, 100)$
MAROON-X Red RV slope ($\text{km s}^{-1} \text{ d}^{-2}$)	$\dot{\gamma}_{1;\text{Red}}$	0.000037 ± 0.000019	$\mathcal{U}(-100, 100)$
Derived Planet <i>b</i> Parameters			
Semi-major axis <i>b</i> over host radius	a_b/R_\star	$16.17^{+0.19}_{-0.20}$	—
Semi-major axis	a_b (AU)	0.0702 ± 0.0012	—
Mass	M_b (M_\oplus)	26.1 ± 1.9	—
Radius	R_b (R_\oplus)	8.10 ± 0.17	—
Companion density	ρ_b (cgs)	$0.269^{+0.028}_{-0.024}$	—
Eccentricity	e	$0.032^{+0.034}_{-0.022}$	—
Orbital Inclination	i_b (deg)	$87.295^{+0.072}_{-0.076}$	—
Mass ratio ($M_{\text{pl.}}/M_\star$)	q	0.0000860 ± 0.0000056	—
Impact parameter	b	$0.763^{+0.021}_{-0.035}$	—
Total transit duration	$T_{\text{tot};b}$ (h)	$2.545^{+0.033}_{-0.028}$	—
Companion surface gravity	g_b (cgs)	394^{+31}_{-26}	—
Equilibrium temperature <i>b</i>	$T_{\text{eq};b}$ (K)	863.9 ± 9.8	—
Insolation Flux	S_{inc} (S_\oplus)	134.7 ± 10	—
Limb darkening coeff.	$u_{1;\text{TESS}}$	$0.42^{+0.27}_{-0.24}$	—
Limb darkening coeff.	$u_{2;\text{TESS}}$	$0.05^{+0.38}_{-0.30}$	—

Exoplanets in this region are extremely important, as they allow us to explore the properties of planets that have not undergone run-away gas accretion.

When compared with planets in wide binary systems, TOI-1173 A *b* is the only low-density super Neptune reported to date. The fundamental parameters of this sample of planet-hosting wide binaries were estimated using high resolution ($R > 50,000$) and high signal-to-noise ratio ($\text{SNR} > 200$) spectroscopy. They represent the best-characterized sample at present, for which precise masses and radii have been obtained through both radial velocity and transit observations. These exoplanets are: WASP-3 A *b* (Bonomo et al. 2017; Behrard et al. 2023), HAT-P-1 B *b* (Turner et al. 2016; Liu

et al. 2014), WASP-94 A *b* (Neveu-VanMalle et al. 2014; Teske et al. 2016), HD 80606 *b* (Bonomo et al. 2017; Behrard et al. 2023), WASP-160 B *b* (Lendl et al. 2019; Jofré et al. 2021), WASP-127 A *b* (Seidel et al. 2020; Behrard et al. 2023), HAT-P-4 *b* (Bonomo et al. 2017; Saffe et al. 2017), HD 202772 A *b* (Wang et al. 2019; Behrard et al. 2023), Kepler-25 B *b* and *c* (Mills et al. 2019; Behrard et al. 2023), KELT-2 A *b* (Stassun et al. 2017; Behrard et al. 2023), XO-2N *b* (Bonomo et al. 2017; Teske et al. 2015), WASP-173 *b* (Labadie-Bartz et al. 2019; Behrard et al. 2023), WASP-180 A *b* (Temple et al. 2019; Behrard et al. 2023), and WASP-64 *b* (Bonomo et al. 2017; Behrard et al. 2023). Only two of these exoplanets have a mass below $20 M_\oplus$, but with

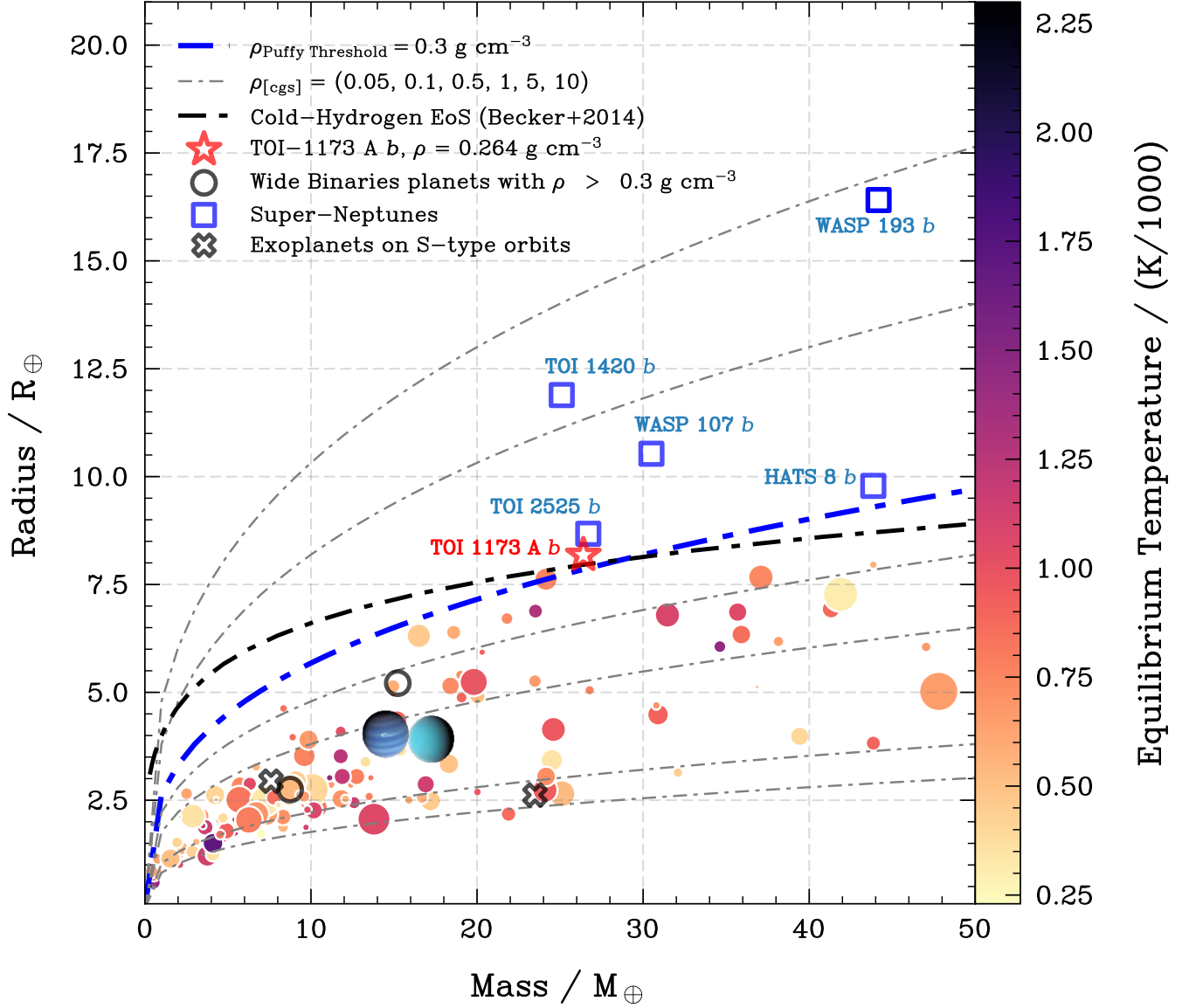


Figure 5. Mass-Radius (M-R) distribution (colored by the planet’s equilibrium temperature and sized by the orbital eccentricity) for confirmed exoplanets presented in the Encyclopædia of Exoplanetary Systems (<https://exoplanet.eu/home/>) as of March 2024. The red star represents TOI-1173 A *b*, and the dashed black line is the theoretical M-R curve for a planet composed of cold Hydrogen according to the H-REOS.3 equation of state from Becker et al. (2014), for which TOI-1173 A *b*’s composition seems to be alike. Constant density curves are shown with dot-dashed lines, and the blue one represents the density threshold adopted in this work for puffy planets. In terms of period, semi-major axis, and mass, TOI-1173 A *b* is similar to TOI-1420 *b* and WASP-107 *b*. The black open circles represent the planets from the wide binary sample with densities higher than 0.3 g cm^{-3} , while black crosses represent planets on S-type orbits (planets that orbit just one star in a binary pair) with masses between $5 - 35 M_{\oplus}$.

densities $\rho > 0.3 \text{ g cm}^{-3}$, depicted as circles in Fig. 5. Within the super Neptune regime, there exists only one wide binary with two exoplanets, Kepler-25 B *b* and *c*. However, these exoplanets have substantially higher densities ($\rho \geq 0.5 \text{ g cm}^{-3}$). This makes TOI-1173 A *b* a potentially unique target for exploring planet formation in wide binary systems.

In the remainder of this section, we investigate different hypotheses to explain the puffy nature of TOI-1173 A *b*.

4.1.1. Stellar Insolation

It is well known that the inflated radii of some hot Jupiters ($M \geq 0.3 M_{\text{Jup}}$, $P < 10$ days, and $T_{\text{eq}} > 1000 \text{ K}$), are primarily attributed to the high incident stellar

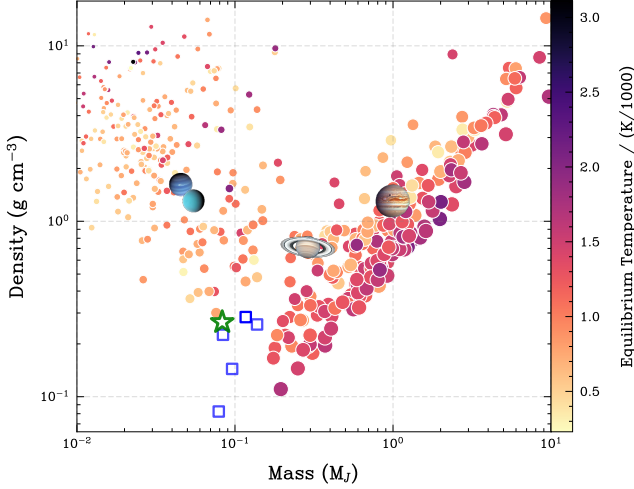


Figure 6. Planetary density as a function of the planetary mass of exoplanets obtained from the Encyclopædia of Exoplanetary Systems as of March 2024. The characteristic “V” shape, and the size of the points, which scale with the planetary radius, denote two regimes of planets. The circles are colored according to their equilibrium temperature. TOI-1173 A *b* (green star) and the other puffy Super-Neptunes (open blue squares) lie in the transition region.

flux upon these planets (e.g., [Batygin & Stevenson 2010](#); [Pu & Valencia 2017](#); [Thorngren & Fortney 2018](#)). A fraction of the light from the star penetrates deep into the planetary atmosphere, where it is then absorbed, causing its inflation (see [Fortney et al. 2021b](#), for more details). However, as seen in Table 4, TOI-1173 A *b* does not share the planetary properties of hot Jupiters, as its insolation and equilibrium temperature are lower.

To ensure a proper comparison with super-Neptunes precisely characterized by transit and RV observations, we have selected stars with temperatures, metallicities, masses, and radii within ± 200 K, ± 0.2 dex, $\pm 0.2 M_{\odot}$, and $\pm 0.2 R_{\odot}$ of those of TOI-1173 A. Figure 7 indicates that the super-Neptune TOI-1173 A *b* and TOI-1420 *b* experience higher incident flux from their host star than other similar gas giants, which suggests that the inflated state of TOI-1173 A *b* could be attributed to stellar insolation. However, assessing whether this insolation is exceptionally high compared to stars with similar properties as TOI-1173 A is challenging due to the restricted sample size.

4.1.2. Excess of Internal Heat

Various studies have highlighted the impact of internal heat on a planet’s radius, indicating that planets with hotter interiors have larger radii and lower densities than those with cooler interiors of the same composition (e.g., [Bodenheimer et al. 2001](#); [Batygin & Stevenson 2010](#); [Lopez & Fortney 2014b](#); [Millholland 2019](#)). This

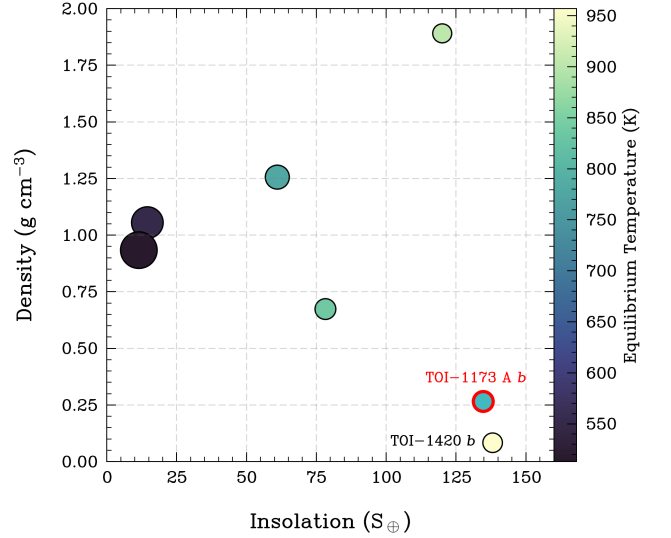


Figure 7. Planet density as a function of stellar insolation. TOI-1173 A *b* is indicated in red. The circles represent the planets with host stars sharing similar physical parameters with TOI-1173 A, colored by their equilibrium temperatures and sized by the planet’s semi-major axis.

inflation stems from the internal heat remaining from the formation of the planet rather than external factors. The age of a planet can influence its internal heat, with younger planets naturally having hotter interiors and consequently larger radii. However, in the case of the ~ 8 billion-year-old TOI-1173 A/B system, TOI-1173 A *b* has already cooled ([Linder et al. 2019](#)). Hence, an alternative mechanism must be responsible for inflating its radius.

4.1.3. Tidal Heating

Tidal heating results from gravitational forces between celestial bodies, causing internal friction and generating heat within the affected body. [Millholland et al. \(2020\)](#) demonstrated that tidal interactions at 0.1 AU can yield tidal luminosities up to $L_{\text{tide}} \sim 10^{29}$ erg s $^{-1}$ (refer to their Figure 1). Applying the tidal luminosity expression from Equation (1) in [Millholland et al. \(2020\)](#), we estimate $L_{\text{tide}} \sim 10^{27}$ erg s $^{-1}$ (assuming zero obliquity and a reduced tidal quality factor $Q' = 10^5$ for Neptune like planets ([Tittlemore & Wisdom 1990](#); [Banfield & Murray 1992](#))) for TOI-1173 A *b*. This suggests the potential for significant tidal heating on the planet.

To further investigate this mechanism, we used the structural model with tidal heating of [Millholland \(2019\)](#). This model incorporates tidal heating effects on planetary structures by considering a two-layer planet model consisting of a heavy element core and an H/He envelope with an MCMC fitting approach. The atmospheric envelope evolution is simulated using the Mod-

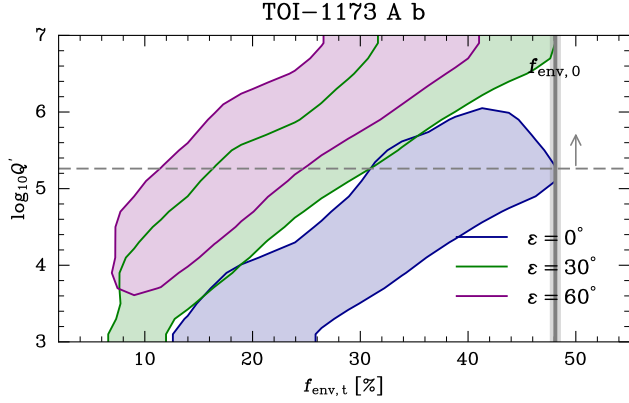


Figure 8. Envelope mass fraction estimates with tides ($f_{\text{env},t}$) and without tides ($f_{\text{env},0}$) of TOI-1173 A *b*. The horizontal dashed lines represent the lower limit of the reduced tidal quality factor ($\log_{10} Q'$). The mean and standard deviation of $f_{\text{env},0}$ are represented by the vertical gray bar. Colored regions indicate the 2σ contours of the posterior distributions of $\log_{10} Q'$ and $f_{\text{env},t}$ after accounting for tides.

ules for Experiments in Stellar Astrophysics (MESA) code (Paxton et al. 2011, 2013, 2018, 2019). Figure 8¹¹ shows the envelope mass fraction estimates for TOI-1173 A *b*. The colored regions indicate the 2D posterior distributions for $\log_{10} Q'$ and $f_{\text{env},t}$ obtained from the fitting that includes tidal inflation. The horizontal dashed lines indicate the lower limit of the reduced tidal quality factor ($\log_{10} Q' \sim 5.2$). These distributions assume the measured eccentricities and indicate the results for obliquity $\epsilon = 0^\circ$, 30° and 60° . The mean and 1σ range of $f_{\text{env},0}$ inferred when neglecting tides are shown with the gray line and bar. The tides-free envelope fraction estimate is $f_{\text{env},0} = 48.1\% \pm 0.4\%$.

Our findings indicate that, when not considering tidal effects, TOI-1173 A *b* has an envelope mass fraction $f_{\text{env},t}$ of approximately $\sim 48\%$. However, incorporating tidal heating into the model led to a significant decrease in the estimated envelope mass fraction, ranging from 10% to 30% for $\epsilon = 30^\circ$ – 60° . This reduction in the envelope mass fraction is attributed to the impact of tidal inflation resulting from eccentricity and obliquity tides. Notably, for $\epsilon = 0^\circ$, the mass fraction would have decrease by 30%, or alternatively, the expanded radius is resolved by including tidal inflation.

4.1.4. Planetary Rings

Piro & Vissapragada (2020) suggested that the inflated radii of low-density puffy planets could be a re-

sult of planetary rings, which would cause deeper-than-expected transits. This hypothesis is contingent upon the rings being at an oblique angle to the planet’s orbital plane. Additionally, if the planet is tidally locked, the impact on the overall transit depth would be negligible. Using the Equation (11) from Piro & Vissapragada (2020), we determined a synchronous timescale of 0.082 Myr for TOI-1173 A *b*, confirming its tidal locking. If TOI-1173 A *b* has rings, they would lie in its orbital plane and thus be observed edge-on from our vantage point, thus not explaining the apparent inflated radius. Moreover, because of the planet’s proximity to its host star, the rings would be susceptible to dissipating or collapsing under various gravitational forces and interactions (Ohta et al. 2009).

4.1.5. Mass Loss by Atmospheric Escape

Given the relatively high stellar irradiation of TOI-1173 A *b* (see Figure 7) and its proximity to its star, it is reasonable to assume that the planet is losing mass. Therefore, the inflated radius may be also attributed to material evaporating and leaving the planet (e.g., Guo 2013; Ehrenreich et al. 2015; Koskinen et al. 2022). Fossati et al. (2017) demonstrated that it is possible to use theoretical models of mass loss to infer whether atmospheric escape is significant on a planet. Using their Equation (10), we computed the restricted Jeans escape parameter as $\Lambda = 28$. Fossati et al. (2017) show in their Fig. 4 that Λ values below the threshold value of $\Lambda_T = 15 - 35$ correspond to significant atmospheric loss. Consequently, TOI-1173 A *b* might be losing its atmosphere. However, it is important to highlight that this possibility is only speculative at the moment given the lack of transmission spectroscopy or multi-band transit photometry for TOI-1173 A *b*. Mass loss measurements are necessary for confirmation, as previously mentioned in Section 1.

4.1.6. Other Causes of the Anomously Large Radius

Alternatively, explanations like high-altitude dust or hazes have been suggested to account for the inflated radii of super-Neptunes (e.g., Wang & Dai 2019; Gao & Zhang 2020b). However, with our current data, it is challenging to confirm if any of these mechanisms could be responsible for inflating the radius of TOI-1173 A *b*, so that transmission spectroscopy is deemed necessary and encouraged for a more conclusive understanding of the planet’s atmospheric physics.

4.2. Dynamical Timescales

In the following, we explore noteworthy features of the interactions between TOI-1173 A and its companion, focusing on turbulent friction, magnetic field main-

¹¹ This figure was generated strictly following the procedure given at <https://github.com/smiholland/Sub-Saturns/>

tenance, and orbital dynamics. When a perturbation occurs, interactions with the primary star can serve as a damping mechanism, effectively obliterating past effects, particularly if these interactions are on a comparable timescale to the age of the system. This phenomenon can be investigated through the consideration of dynamical timescales derived from the mass of the system components (primary star, secondary star, and the planet), the degree of tidal detachment, and their respective orbital eccentricities.

4.2.1. Realignment due to Turbulent Friction

With an effective temperature of $T_{\text{eff}} = 5350 \pm 34$ K, TOI-1173 A lies well below the Kraft Break (KB; Kraft 1967), a boundary that separates stars with deep convective envelopes and efficient magnetic dynamos from those without ($T_{\text{eff,KB}} < 6200$ K). Our estimate of TOI-1173 A's convective mass, which yielded a value of $0.0537 M_{\odot}$ (more details in Yana Galarza et al., 2024, submitted), also supports this claim. Given its substantial ability to maintain a magnetic field, realignment between the star's rotation and the planet's orbit is expected to be more efficient, slowing down through magnetic braking.

For such stars, the empirical tidal realignment timescale can be estimated as

$$\tau_{\text{CE}} = 10^{10} q^{-2} \left(\frac{a/R_{\star}}{40} \right)^6, \quad (2)$$

calibrated from observations made in binary star systems by Zahn (1977). Here, q represents the mass ratio of the companion to the host star (M_b/M_{\star}), and a/R_{\star} its level of tidal detachment¹² (Albrecht et al. 2012). For TOI-1173 A b , we found $\tau_{\text{CE}} \sim 10^{15}$ years, and a comparison with the proper system's age ($\Gamma \sim 8.7 \times 10^9$ years) indicates that the planet's spin-orbit orientation likely has not changed since its initial formation.

Nevertheless, whether the system was born aligned or not is uncertain with current data, and TOI-1173 A b represents a benchmark follow-up case for further analysis via the Rossiter-McLaughlin (RM) effect. As a spin-orbit aligned occulter transits, it initially obscures the blue-shifted hemisphere of a star, followed by the observation of the red-shifted hemisphere (Holt 1893). Any asymmetries in the RM profile suggest misalignment between the orbital plane and the host star's equator, indicating either a system that did not form in a flat disc or one that experienced dynamical perturbations after disc

dispersal (Winn & Fabrycky 2015). Following the framework in Triaud (2018), we estimated an expected RM amplitude of $\sim 4 \text{ m s}^{-1}$ for TOI-1173 A b , so that the system could be observed with current extreme-precision spectrographs such as the Keck Planet Finder (KPF; Gibson et al. 2016), the EXtreme PREcision Spectrometer (EXPRES; Blackman et al. 2020) and so on.

4.2.2. Eccentricity Driven by Tidal Dissipation

For comparison with the system's tidal realignment timescale, we also consider the evolution timescale of TOI-1173 A b 's orbital eccentricity $\tau_e \sim e/(de/dt)$. Assuming that the planet is in pseudo-synchronous rotation, its energy dissipation rate can be expressed as

$$\dot{e} = \left[\frac{21\kappa_2 G M^2 \Omega R^5 \zeta(e)}{2Q' a^6} \right] \frac{a(1-e^2)}{GMme}, \quad (3)$$

where \dot{e} is in s^{-1} and Ω is the pseudo-synchronous rotation rate that, similar to the corrective factor $\zeta(e)$, depends on the companion's eccentricity and orbital period in the form (Hut 1981; Wisdom 2008):

$$\Omega = \frac{1}{P} \left[\frac{f_1(e)}{f_2(e)\beta^3} \right], \text{ with } \beta \equiv \sqrt{1-e^2}, \quad (4)$$

$$\zeta(e) = \frac{2}{7} \left[\frac{f_0(e)}{\beta^{15}} - 2 \frac{f_1(e)}{\beta^{12}} + \frac{f_2(e)}{\beta^9} \right], \quad (5)$$

and,

$$f_0(e) = 1 + \frac{31}{2}e^2 + \frac{255}{8}e^4 + \frac{185}{16}e^6 + \frac{25}{64}e^8, \quad (6)$$

$$f_1(e) = 1 + \frac{15}{2}e^2 + \frac{45}{8}e^4 + \frac{5}{16}e^6, \quad (7)$$

$$f_2(e) = 1 + 3e^2 + \frac{3}{8}e^4. \quad (8)$$

We derived an eccentricity of 0.032 for TOI-1173 A b (refer to Section 3), and it is worth noting that, over time, planets are anticipated to circularise their orbits especially due to energy loss caused by tidal dissipation (Dawson & Johnson 2018). Using a tidal dissipation parameter within the range $Q' = 10^4 - 10^6$ and adopting $\kappa_2 = 0.3$ as the Love number based on Penev et al. (2018) and Rice et al. (2022), which represents the companion's rigidity and susceptibility to changes in shape in response to a tidal potential, we calculated a tidal circularization timescale of $\tau_e \approx 10^9 - 10^{11}$ years for TOI-1173 A b .

We note that the value of Q' in this range is also supported by the results obtained in Subsec. 4.1.2 using the tidal heating model of Millholland et al. (2020).

Relative to the system's age, the tidal circularization timescale could be as short as 1 Gyr, which is much less

¹² Tidal detachment determines whether a planet undergoes tidal interactions with the host star (for more details see Rice et al. 2023).

than the age of the planet ($\Gamma \sim 8.7$ Gyr). Therefore, it is plausible that TOI-1173 A *b* may have exhibited a higher eccentricity in the past, and it was subsequently dampened after a few billion years. On the other hand, the circularization timescale may also be much longer, in which case no evolution in eccentricity over the planet’s lifetime would be expected. Since the derived eccentricity of TOI-1173 A *b* today is consistent with zero at the 1.5σ level, we cannot draw strong conclusions about the original eccentricity of its orbit at formation.

4.2.3. Perturbations due to a Tertiary Companion

Under a quadrupole level of approximation, a planet’s orbit has the potential to adopt a low-eccentricity arrangement through von-Zeipel-Lidov-Kozai (vZLK) cycles due to interactions with a tertiary companion. This ensures the conservation of the system’s angular momentum vector component along the z -axis, and in the context of a hierarchical triple-body system, where the planet’s mass is considerably smaller than the proper masses of the binary stars, the timescale for the vZLK process can be determined from the equation

$$\tau_{\text{vZLK}} \sim \frac{16}{30\pi} \left(\frac{P_B^2}{P_b} \right) (1 - e_B^2)^{3/2} \left(\frac{M_A + M_B}{M_B} \right), \quad (9)$$

where e_B , M_B , and P_B are the orbital eccentricity, mass and period of the tertiary companion, and P_b is the planet’s period (Naoz 2016).

The eccentricity for TOI-1173 A/B system is uncertain, therefore, to estimate τ_{vZLK} , we considered e_B ranging from 0.0 to 0.9. At the current architecture, we estimated the timescale for vZLK perturbations in the order of $\tau_{\text{vZLK}, e=0} \sim 10^{13}$ years, and $\tau_{\text{vZLK}, e=0.9} \sim 10^{12}$ years. Comparing those parameters with the system’s age, we observed that the timescale is bigger than Γ , even comparable to the age of the Universe, indicating that vZLK migration might not have significantly influenced the system’s evolution if TOI-1173 A *b* originated near its present location, i.e., its damping timescale is sufficiently large to be unobserved. Interestingly, when extrapolating its initial position for $P_b = 1$ year, a Jupiter-like current location with $P_b \sim 12$ years, or Saturn-like with $P_b \sim 30$ years, τ_{vZLK} ranges between $\sim 10^{11}$ and $\sim 10^8$ years. If the planet initially formed far away from its current position, consistent with theories of giant planet formation (D’Angelo & Lubow 2008; Batygin & Laughlin 2015, and references therein), τ_{vZLK} approaches Γ , indicating the possibility of past migration through vZLK mechanisms.

4.2.4. Apsidal Precession due to General Relativity

vZLK oscillations can be however dampened by additional perturbations that induce apsidal precession at a faster rate, thereby diminishing the orbit-averaged torque exerted by the companion star (Wu & Murray 2003; Rice et al. 2023). As for apsidal precession arising from general relativity, the dampening timescale is given by

$$\tau_{\text{GR}} = \frac{2\pi c^2}{3(GM)^{3/2}} (1 - e_b^2) a_b^{5/2}. \quad (10)$$

For TOI-1173 A *b* we estimated $\tau_{\text{GR}} \sim 10^4$ years; a short timescale when compared to both τ_{vZLK} and the system’s age. This effectively eliminates the possibility of the system undergoing vZLK oscillations, as the influence of general relativity on apsidal precession is substantially faster when compared to the system’s age.

5. CONCLUSIONS AND FUTURE WORK

We present the discovery of TOI-1173 A *b*, the first super-Neptune ($M = 26.1M_{\oplus}$) with a highly inflated radius ($R = 8.10R_{\oplus}$) in a wide binary system (separation ~ 11400 AU). TESS photometry and radial velocity observations with the MAROON-X spectrograph at Gemini North revealed a planet on a nearly circular ($e = 0.032$) close-in orbit ($P = 7.064$ days, $a = 0.062$ au) to the primary star. Additionally, we infer a density of $\rho = 0.269 \text{ g cm}^{-3}$, equilibrium temperature $T_{\text{eq}} = 863$ K and insolation flux $S_{\oplus} = 134.7$ for the planet. TOI-1173 A *b* stands out as the only low-density super Neptune in a binary system reported to date.

Hypotheses exploring the causes of the planet’s inflated nature include stellar insolation, excess internal heat, presence of planetary rings, and the potential mass loss by atmospheric escape. Although stellar insolation, internal heat and mass loss may contribute (see Subsection 4.1), we highlighted the negligible impact of planetary rings due to the planet’s tidally locked nature. Therefore, we conclude that the most promising scenario to explain the inflated radius of TOI-1173 A *b* is tidal heating.

We investigated the dynamical evolution of TOI-1173 A and its planetary companion, examining factors such as realignment due to turbulent friction with the star, eccentricity evolution influenced by tidal dissipation, the impact of tertiary companions, and the role of general relativity-induced apsidal precession (see Subsection 4.2). Our findings suggest that TOI-1173 A *b* likely formed stably and has maintained its stability over time ($\tau_{\text{CE}} \gg \Gamma$), however, the alignment of the system remains uncertain, and further analysis is required and encouraged in this aspect. Other than direct RM observations (Ohta et al. 2005), gravity darkening (Ahlers

et al. 2020), and interferometry (Le Bouquin et al. 2009) can be also used for spin-orbit analyses.

The comparability between the tidal circularization timescale and the system’s age, expressed as $\tau_e \sim \Gamma$, leaves us without a clear conclusion on whether the system exhibited a high eccentricity in the past. Under these highly eccentric configurations, other possible formation mechanisms include single planet-planet scattering events (e.g., Rasio & Ford 1996; Chatterjee et al. 2008), and resonant interactions (Naoz et al. 2011; Petrovich & Tremaine 2016), while low-eccentricities are usually associated to high multiplicity, as in our own Solar System (e.g., Lissauer 1993; Ford & Rasio 2008; Limbach & Turner 2015; Van Eylen & Albrecht 2015), or smooth disc migration (Goldreich & Sari 2003; Lega et al. 2021). With $\tau_{\text{vZLK}} > \Gamma$, TOI-1173 A b might have undergone migration through this mechanism, however, the possibility of current vZLK oscillations occurring in the system is eliminated given that the apsidal precession timescale due to general relativity is orders of magnitude smaller than the proper vZLK timescale ($\tau_{\text{GR}} \ll \tau_{\text{vZLK}}$).

Looking ahead, the low mass and density of TOI-1173 A b, along with TOI-2525 b, WASP-107 b, TOI-1420 b, HATS-8 b, and WASP-193 b, make it a key planet for atmospheric and dynamical characterization, with further analysis necessary and encouraged to uncover its extreme atmospheric physics in details, as well as to reveal its past orbital configuration.

ACKNOWLEDGMENTS

Jhon Yana Galarza acknowledges support from a Carnegie Fellowship. Thiago Ferreira acknowledges support from Yale Graduate School of Arts and Sciences. Diego Lorenzo Oliveira acknowledges support from CNPq (PCI 301612/2024-2). Henrique Reggiani acknowledges the support from NOIRLab, which is managed by the Association of Universities for Research in Astronomy (AURA) under a cooperative agreement with the National Science Foundation.

This work made use of data collected with the Gemini Telescope. This paper includes data collected by the TESS mission. Funding for the TESS mission

is provided by NASA’s Science Mission Directorate. This research has made use of the Exoplanet Follow-up Observation Program (ExoFOP; DOI: 10.26134/ExoFOP5) website, which is operated by the California Institute of Technology, under contract with the National Aeronautics and Space Administration under the Exoplanet Exploration Program. Some of the data presented herein were obtained at Keck Observatory, which is a private 501(c)3 non-profit organization operated as a scientific partnership among the California Institute of Technology, the University of California, and the National Aeronautics and Space Administration. The Observatory was made possible by the generous financial support of the W. M. Keck Foundation. The authors wish to recognize and acknowledge the very significant cultural role and reverence that the summit of Maunakea has always had within the Native Hawaiian community. We are most fortunate to have the opportunity to conduct observations from this mountain. Some of the data presented in this paper were obtained from the Mikulski Archive for Space Telescopes (MAST) at the Space Telescope Science Institute. The specific observations analyzed can be accessed via <http://dx.doi.org/10.17909/dpx3-gv19>. STScI is operated by the Association of Universities for Research in Astronomy, Inc., under NASA contract NAS5-26555. Support to MAST for these data is provided by the NASA Office of Space Science via grant NAG5-7584 and by other grants and contracts.

Facilities: Gemini, TESS, The Encyclopædia of Exoplanetary Systems, The Exoplanet Follow-up Observation Program.

Software: NUMPY (van der Walt et al. 2011), MATPLOTLIB (Hunter 2007), PANDAS (McKinney 2010), LIGHTKKURVE (Lightkurve Collaboration et al. 2018), SCIPY (Virtanen et al. 2020), JULIET (Espinoza et al. 2019), ASTROML (Ivezić et al. 2014), DYNESTY (Speagle 2020), ALLESFITTER (Günther & Daylan 2021), ASTROBASE (Bhatti et al. 2021), SERVAL (Zechmeister et al. 2020), MESA (Paxton et al. 2019), EMCEE (Foreman-Mackey et al. 2013), SUB-SATURNS (Millholland et al. 2020), SMPLOTLIB (Li 2023).

REFERENCES

- Ahlers, J. P., Kruse, E., Colón, K. D., et al. 2020, ApJ, 888, 63, doi: [10.3847/1538-4357/ab59d0](https://doi.org/10.3847/1538-4357/ab59d0)
- Albrecht, S., Winn, J. N., Johnson, J. A., et al. 2012, ApJ, 757, 18, doi: [10.1088/0004-637X/757/1/18](https://doi.org/10.1088/0004-637X/757/1/18)
- Anderson, D. R., Collier Cameron, A., Delrez, L., et al. 2017, A&A, 604, A110, doi: [10.1051/0004-6361/201730439](https://doi.org/10.1051/0004-6361/201730439)
- Banfield, D., & Murray, N. 1992, Icarus, 99, 390, doi: [10.1016/0019-1035\(92\)90155-Z](https://doi.org/10.1016/0019-1035(92)90155-Z)

- Barkaoui, K., Pozuelos, F. J., Hellier, C., et al. 2023, arXiv e-prints, arXiv:2307.08350, doi: [10.48550/arXiv.2307.08350](https://doi.org/10.48550/arXiv.2307.08350)
- Batygin, K., & Laughlin, G. 2015, *Proceedings of the National Academy of Science*, 112, 4214, doi: [10.1073/pnas.1423252112](https://doi.org/10.1073/pnas.1423252112)
- Batygin, K., & Stevenson, D. J. 2010, *ApJL*, 714, L238, doi: [10.1088/2041-8205/714/2/L238](https://doi.org/10.1088/2041-8205/714/2/L238)
- Bayliss, D., Hartman, J. D., Bakos, G. Á., et al. 2015, *AJ*, 150, 49, doi: [10.1088/0004-6256/150/2/49](https://doi.org/10.1088/0004-6256/150/2/49)
- Becker, A., Lorenzen, W., Fortney, J. J., et al. 2014, *ApJS*, 215, 21, doi: [10.1088/0067-0049/215/2/21](https://doi.org/10.1088/0067-0049/215/2/21)
- Behrard, A., Dai, F., Brewer, J. M., Berger, T. A., & Howard, A. W. 2023, *MNRAS*, 521, 2969, doi: [10.1093/mnras/stad745](https://doi.org/10.1093/mnras/stad745)
- Bennett, K. A., Redfield, S., Oklopčić, A., et al. 2023, *AJ*, 165, 264, doi: [10.3847/1538-3881/acd34b](https://doi.org/10.3847/1538-3881/acd34b)
- Bhatti, W., Bouma, L., Joshua, et al. 2021, waqasbhatti/astrobases: astrobases v0.5.3, v0.5.3, Zenodo, doi: [10.5281/zenodo.4445344](https://doi.org/10.5281/zenodo.4445344)
- Bitsch, B., Lambrechts, M., & Johansen, A. 2015, *A&A*, 582, A112, doi: [10.1051/0004-6361/201526463](https://doi.org/10.1051/0004-6361/201526463)
- Blackman, R. T., Fischer, D. A., Jurgenson, C. A., et al. 2020, *AJ*, 159, 238, doi: [10.3847/1538-3881/ab811d](https://doi.org/10.3847/1538-3881/ab811d)
- Bodenheimer, P., Lin, D. N. C., & Mardling, R. A. 2001, *ApJ*, 548, 466, doi: [10.1086/318667](https://doi.org/10.1086/318667)
- Bonomo, A. S., Desidera, S., Benatti, S., et al. 2017, *A&A*, 602, A107, doi: [10.1051/0004-6361/201629882](https://doi.org/10.1051/0004-6361/201629882)
- Cauley, P. W., Redfield, S., & Jensen, A. G. 2017, *AJ*, 153, 217, doi: [10.3847/1538-3881/aa6a15](https://doi.org/10.3847/1538-3881/aa6a15)
- Chatterjee, S., Ford, E. B., Matsumura, S., & Rasio, F. A. 2008, *ApJ*, 686, 580, doi: [10.1086/590227](https://doi.org/10.1086/590227)
- Christie, D., Arras, P., & Li, Z.-Y. 2013, *ApJ*, 772, 144, doi: [10.1088/0004-637X/772/2/144](https://doi.org/10.1088/0004-637X/772/2/144)
- Ciardi, D. R., Beichman, C. A., Horch, E. P., & Howell, S. B. 2015, *ApJ*, 805, 16, doi: [10.1088/0004-637X/805/1/16](https://doi.org/10.1088/0004-637X/805/1/16)
- D’Angelo, G., & Lubow, S. H. 2008, *ApJ*, 685, 560, doi: [10.1086/590904](https://doi.org/10.1086/590904)
- Dawson, R. I., & Johnson, J. A. 2018, *ARA&A*, 56, 175, doi: [10.1146/annurev-astro-081817-051853](https://doi.org/10.1146/annurev-astro-081817-051853)
- Doazan, V., & Peton, A. 1970, *A&A*, 9, 245
- dos Santos, L. A., Ehrenreich, D., Bourrier, V., et al. 2020, *A&A*, 640, A29, doi: [10.1051/0004-6361/202038802](https://doi.org/10.1051/0004-6361/202038802)
- Ehrenreich, D., Bourrier, V., Wheatley, P. J., et al. 2015, *Nature*, 522, 459, doi: [10.1038/nature14501](https://doi.org/10.1038/nature14501)
- Espinoza, N., & Jordán, A. 2016, *MNRAS*, 457, 3573, doi: [10.1093/mnras/stw224](https://doi.org/10.1093/mnras/stw224)
- Espinoza, N., Kossakowski, D., & Brahm, R. 2019, *MNRAS*, 490, 2262, doi: [10.1093/mnras/stz2688](https://doi.org/10.1093/mnras/stz2688)
- Ford, E. B., & Rasio, F. A. 2008, *ApJ*, 686, 621, doi: [10.1086/590926](https://doi.org/10.1086/590926)
- Foreman-Mackey, D., Hogg, D. W., Lang, D., & Goodman, J. 2013, *PASP*, 125, 306, doi: [10.1086/670067](https://doi.org/10.1086/670067)
- Fortney, J. J., Dawson, R. I., & Komacek, T. D. 2021a, *Journal of Geophysical Research (Planets)*, 126, e06629, doi: [10.1029/2020JE006629](https://doi.org/10.1029/2020JE006629)
- . 2021b, *Journal of Geophysical Research (Planets)*, 126, e06629, doi: [10.1029/2020JE006629](https://doi.org/10.1029/2020JE006629)
- Fossati, L., Erkaev, N. V., Lammer, H., et al. 2017, *A&A*, 598, A90, doi: [10.1051/0004-6361/201629716](https://doi.org/10.1051/0004-6361/201629716)
- Gao, P., & Zhang, X. 2020a, *ApJ*, 890, 93, doi: [10.3847/1538-4357/ab6a9b](https://doi.org/10.3847/1538-4357/ab6a9b)
- . 2020b, *ApJ*, 890, 93, doi: [10.3847/1538-4357/ab6a9b](https://doi.org/10.3847/1538-4357/ab6a9b)
- Gibson, S. R., Howard, A. W., Marcy, G. W., et al. 2016, in *Society of Photo-Optical Instrumentation Engineers (SPIE) Conference Series*, Vol. 9908, *Ground-based and Airborne Instrumentation for Astronomy VI*, ed. C. J. Evans, L. Simard, & H. Takami, 990870, doi: [10.1117/12.2233334](https://doi.org/10.1117/12.2233334)
- Goldreich, P., & Sari, R. 2003, *ApJ*, 585, 1024, doi: [10.1086/346202](https://doi.org/10.1086/346202)
- Guerrero, N. M., Seager, S., Huang, C. X., et al. 2021, *ApJS*, 254, 39, doi: [10.3847/1538-4365/abef1](https://doi.org/10.3847/1538-4365/abef1)
- Günther, M. N., & Daylan, T. 2021, *ApJS*, 254, 13, doi: [10.3847/1538-4365/abe70e](https://doi.org/10.3847/1538-4365/abe70e)
- Guo, J. H. 2013, *ApJ*, 766, 102, doi: [10.1088/0004-637X/766/2/102](https://doi.org/10.1088/0004-637X/766/2/102)
- Holt, J. R. 1893, *Astronomy and Astro-Physics (formerly The Sidereal Messenger)*, 12, 646
- Hunter, J. D. 2007, *Computing in Science Engineering*, 9, 90, doi: [10.1109/MCSE.2007.55](https://doi.org/10.1109/MCSE.2007.55)
- Hut, P. 1981, *A&A*, 99, 126
- Ida, S., & Lin, D. N. C. 2004, *ApJ*, 604, 388, doi: [10.1086/381724](https://doi.org/10.1086/381724)
- Ivezić, Ž., Connolly, A. J., VanderPlas, J. T., & Gray, A. 2014, *Statistics, Data Mining, and Machine Learning in Astronomy: A Practical Python Guide for the Analysis of Survey Data*, doi: [10.1515/9781400848911](https://doi.org/10.1515/9781400848911)
- Jenkins, J. M., Twicken, J. D., McCauliff, S., et al. 2016, in *Society of Photo-Optical Instrumentation Engineers (SPIE) Conference Series*, Vol. 9913, *Software and Cyberinfrastructure for Astronomy IV*, ed. G. Chiozzi & J. C. Guzman, 99133E, doi: [10.1117/12.2233418](https://doi.org/10.1117/12.2233418)
- Jensen, A. G., Redfield, S., Endl, M., et al. 2012, *ApJ*, 751, 86, doi: [10.1088/0004-637X/751/2/86](https://doi.org/10.1088/0004-637X/751/2/86)
- Jofré, E., Petrucci, R., Maqueo Chew, Y. G., et al. 2021, *AJ*, 162, 291, doi: [10.3847/1538-3881/ac25ef](https://doi.org/10.3847/1538-3881/ac25ef)
- Kipping, D. M. 2013, *MNRAS*, 435, 2152, doi: [10.1093/mnras/stt1435](https://doi.org/10.1093/mnras/stt1435)

- Kislyakova, K. G., Holmström, M., Odert, P., et al. 2019, *A&A*, 623, A131, doi: [10.1051/0004-6361/201833941](https://doi.org/10.1051/0004-6361/201833941)
- Koskinen, T. T., Lavvas, P., Huang, C., et al. 2022, *ApJ*, 929, 52, doi: [10.3847/1538-4357/ac4f45](https://doi.org/10.3847/1538-4357/ac4f45)
- Kovács, G., Zucker, S., & Mazeh, T. 2002, *A&A*, 391, 369, doi: [10.1051/0004-6361:20020802](https://doi.org/10.1051/0004-6361:20020802)
- Kraft, R. P. 1967, *ApJ*, 150, 551, doi: [10.1086/149359](https://doi.org/10.1086/149359)
- Krolikowski, D. M., Kraus, A. L., Tofflemire, B. M., et al. 2024, *AJ*, 167, 79, doi: [10.3847/1538-3881/ad0f22](https://doi.org/10.3847/1538-3881/ad0f22)
- Labadie-Bartz, J., Rodriguez, J. E., Stassun, K. G., et al. 2019, *ApJS*, 240, 13, doi: [10.3847/1538-4365/aaee7e](https://doi.org/10.3847/1538-4365/aaee7e)
- Le Bouquin, J. B., Absil, O., Benisty, M., et al. 2009, *A&A*, 498, L41, doi: [10.1051/0004-6361/200911854](https://doi.org/10.1051/0004-6361/200911854)
- Lee, E. J., & Chiang, E. 2015, *ApJ*, 811, 41, doi: [10.1088/0004-637X/811/1/41](https://doi.org/10.1088/0004-637X/811/1/41)
- Lega, E., Nelson, R. P., Morbidelli, A., et al. 2021, *A&A*, 646, A166, doi: [10.1051/0004-6361/202039520](https://doi.org/10.1051/0004-6361/202039520)
- Lendl, M., Anderson, D. R., Bonfanti, A., et al. 2019, *MNRAS*, 482, 301, doi: [10.1093/mnras/sty2667](https://doi.org/10.1093/mnras/sty2667)
- Li, J. 2023, *AstroJacobLi/smplotlib: v0.0.9, v0.0.9*, Zenodo, doi: [10.5281/zenodo.8126529](https://doi.org/10.5281/zenodo.8126529)
- Lightkurve Collaboration, Cardoso, J. V. d. M., Hedges, C., et al. 2018, *Lightkurve: Kepler and TESS time series analysis in Python*, *Astrophysics Source Code Library*, record ascl:1812.013
- Limbach, M. A., & Turner, E. L. 2015, *Proceedings of the National Academy of Science*, 112, 20, doi: [10.1073/pnas.1406545111](https://doi.org/10.1073/pnas.1406545111)
- Linder, E. F., Mordasini, C., Mollière, P., et al. 2019, *A&A*, 623, A85, doi: [10.1051/0004-6361/201833873](https://doi.org/10.1051/0004-6361/201833873)
- Lissauer, J. J. 1993, *ARA&A*, 31, 129, doi: [10.1146/annurev.aa.31.090193.001021](https://doi.org/10.1146/annurev.aa.31.090193.001021)
- Lissauer, J. J., & Stewart, G. R. 1993, in *Protostars and Planets III*, ed. E. H. Levy & J. I. Lunine, 1061
- Liu, F., Asplund, M., Ramirez, I., Yong, D., & Melendez, J. 2014, *MNRAS*, 442, L51, doi: [10.1093/mnrasl/slu055](https://doi.org/10.1093/mnrasl/slu055)
- Lopez, E. D., & Fortney, J. J. 2014a, *ApJ*, 792, 1, doi: [10.1088/0004-637X/792/1/1](https://doi.org/10.1088/0004-637X/792/1/1)
- . 2014b, *ApJ*, 792, 1, doi: [10.1088/0004-637X/792/1/1](https://doi.org/10.1088/0004-637X/792/1/1)
- Lucy, L. B., & Sweeney, M. A. 1971, *AJ*, 76, 544, doi: [10.1086/111159](https://doi.org/10.1086/111159)
- Mayor, M., & Queloz, D. 1995, *Nature*, 378, 355, doi: [10.1038/378355a0](https://doi.org/10.1038/378355a0)
- McKinney, W. 2010, in *Proceedings of the 9th Python in Science Conference*, ed. S. van der Walt & J. Millman, 51 – 56
- Millholland, S. 2019, *ApJ*, 886, 72, doi: [10.3847/1538-4357/ab4c3f](https://doi.org/10.3847/1538-4357/ab4c3f)
- Millholland, S., Petigura, E., & Batygin, K. 2020, *ApJ*, 897, 7, doi: [10.3847/1538-4357/ab959c](https://doi.org/10.3847/1538-4357/ab959c)
- Mills, S. M., Howard, A. W., Weiss, L. M., et al. 2019, *AJ*, 157, 145, doi: [10.3847/1538-3881/ab0899](https://doi.org/10.3847/1538-3881/ab0899)
- Mugrauer, M., Ginski, C., & Seeliger, M. 2014, *MNRAS*, 439, 1063, doi: [10.1093/mnras/stu044](https://doi.org/10.1093/mnras/stu044)
- Murray-Clay, R. A., Chiang, E. I., & Murray, N. 2009, *ApJ*, 693, 23, doi: [10.1088/0004-637X/693/1/23](https://doi.org/10.1088/0004-637X/693/1/23)
- Naoz, S. 2016, *ARA&A*, 54, 441, doi: [10.1146/annurev-astro-081915-023315](https://doi.org/10.1146/annurev-astro-081915-023315)
- Naoz, S., Farr, W. M., Lithwick, Y., Rasio, F. A., & Teyssandier, J. 2011, *Nature*, 473, 187, doi: [10.1038/nature10076](https://doi.org/10.1038/nature10076)
- Neveu-VanMalle, M., Queloz, D., Anderson, D. R., et al. 2014, *A&A*, 572, A49, doi: [10.1051/0004-6361/201424744](https://doi.org/10.1051/0004-6361/201424744)
- Ohno, K., & Tanaka, Y. A. 2021, *ApJ*, 920, 124, doi: [10.3847/1538-4357/ac1516](https://doi.org/10.3847/1538-4357/ac1516)
- Ohta, Y., Taruya, A., & Suto, Y. 2005, *ApJ*, 622, 1118, doi: [10.1086/428344](https://doi.org/10.1086/428344)
- . 2009, *ApJ*, 690, 1, doi: [10.1088/0004-637X/690/1/1](https://doi.org/10.1088/0004-637X/690/1/1)
- Orell-Miquel, J., Murgas, F., Pallé, E., et al. 2022, *A&A*, 659, A55, doi: [10.1051/0004-6361/202142455](https://doi.org/10.1051/0004-6361/202142455)
- Owen, J. E., & Wu, Y. 2013, *ApJ*, 775, 105, doi: [10.1088/0004-637X/775/2/105](https://doi.org/10.1088/0004-637X/775/2/105)
- Owen, J. E., Murray-Clay, R. A., Schreyer, E., et al. 2023, *MNRAS*, 518, 4357, doi: [10.1093/mnras/stac3414](https://doi.org/10.1093/mnras/stac3414)
- Paxton, B., Bildsten, L., Dotter, A., et al. 2011, *ApJS*, 192, 3, doi: [10.1088/0067-0049/192/1/3](https://doi.org/10.1088/0067-0049/192/1/3)
- Paxton, B., Cantiello, M., Arras, P., et al. 2013, *ApJS*, 208, 4, doi: [10.1088/0067-0049/208/1/4](https://doi.org/10.1088/0067-0049/208/1/4)
- Paxton, B., Schwab, J., Bauer, E. B., et al. 2018, *ApJS*, 234, 34, doi: [10.3847/1538-4365/aaa5a8](https://doi.org/10.3847/1538-4365/aaa5a8)
- Paxton, B., Smolec, R., Schwab, J., et al. 2019, *ApJS*, 243, 10, doi: [10.3847/1538-4365/ab2241](https://doi.org/10.3847/1538-4365/ab2241)
- Penev, K., Bouma, L. G., Winn, J. N., & Hartman, J. D. 2018, *AJ*, 155, 165, doi: [10.3847/1538-3881/aaaf71](https://doi.org/10.3847/1538-3881/aaaf71)
- Petrovich, C., & Tremaine, S. 2016, *ApJ*, 829, 132, doi: [10.3847/0004-637X/829/2/132](https://doi.org/10.3847/0004-637X/829/2/132)
- Piaulet, C., Benneke, B., Rubenzahl, R. A., et al. 2021, *AJ*, 161, 70, doi: [10.3847/1538-3881/abcd3c](https://doi.org/10.3847/1538-3881/abcd3c)
- Piro, A. L., & Vissapragada, S. 2020, *AJ*, 159, 131, doi: [10.3847/1538-3881/ab7192](https://doi.org/10.3847/1538-3881/ab7192)
- Pollack, J. B., Hubickyj, O., Bodenheimer, P., et al. 1996, *Icarus*, 124, 62, doi: [10.1006/icar.1996.0190](https://doi.org/10.1006/icar.1996.0190)
- Pu, B., & Valencia, D. 2017, *ApJ*, 846, 47, doi: [10.3847/1538-4357/aa826f](https://doi.org/10.3847/1538-4357/aa826f)
- Rasio, F. A., & Ford, E. B. 1996, *Science*, 274, 954, doi: [10.1126/science.274.5289.954](https://doi.org/10.1126/science.274.5289.954)
- Rasmussen, C. E., & Williams, C. K. I. 2006, *Gaussian Processes for Machine Learning*
- Rice, M., Wang, S., Gerbig, K., et al. 2023, *AJ*, 165, 65, doi: [10.3847/1538-3881/aca88e](https://doi.org/10.3847/1538-3881/aca88e)

- Rice, M., Wang, S., & Laughlin, G. 2022, *ApJL*, 926, L17, doi: [10.3847/2041-8213/ac502d](https://doi.org/10.3847/2041-8213/ac502d)
- Rice, W. K. M., & Armitage, P. J. 2003, *ApJL*, 598, L55, doi: [10.1086/380390](https://doi.org/10.1086/380390)
- Ricker, G. R., Winn, J. N., Vanderspek, R., et al. 2015, *Journal of Astronomical Telescopes, Instruments, and Systems*, 1, 014003, doi: [10.1117/1.JATIS.1.1.014003](https://doi.org/10.1117/1.JATIS.1.1.014003)
- Saffe, C., Jofré, E., Martioli, E., et al. 2017, *A&A*, 604, L4, doi: [10.1051/0004-6361/201731430](https://doi.org/10.1051/0004-6361/201731430)
- Seidel, J. V., Lendl, M., Bourrier, V., et al. 2020, *A&A*, 643, A45, doi: [10.1051/0004-6361/202039058](https://doi.org/10.1051/0004-6361/202039058)
- Seifahrt, A., Stürmer, J., Bean, J. L., & Schwab, C. 2018, in *Society of Photo-Optical Instrumentation Engineers (SPIE) Conference Series*, Vol. 10702, *Ground-based and Airborne Instrumentation for Astronomy VII*, ed. C. J. Evans, L. Simard, & H. Takami, 107026D, doi: [10.1117/12.2312936](https://doi.org/10.1117/12.2312936)
- Seifahrt, A., Bean, J. L., Kasper, D., et al. 2022, in *Society of Photo-Optical Instrumentation Engineers (SPIE) Conference Series*, Vol. 12184, *Ground-based and Airborne Instrumentation for Astronomy IX*, ed. C. J. Evans, J. J. Bryant, & K. Motohara, 121841G, doi: [10.1117/12.2629428](https://doi.org/10.1117/12.2629428)
- Sobolev, V. V. 1960, *Moving Envelopes of Stars*, doi: [10.4159/harvard.9780674864658](https://doi.org/10.4159/harvard.9780674864658)
- Spake, J. J., Sing, D. K., Evans, T. M., et al. 2018, *Nature*, 557, 68, doi: [10.1038/s41586-018-0067-5](https://doi.org/10.1038/s41586-018-0067-5)
- Speagle, J. S. 2020, *MNRAS*, 493, 3132, doi: [10.1093/mnras/staa278](https://doi.org/10.1093/mnras/staa278)
- Stassun, K. G., Collins, K. A., & Gaudi, B. S. 2017, *AJ*, 153, 136, doi: [10.3847/1538-3881/aa5df3](https://doi.org/10.3847/1538-3881/aa5df3)
- Temple, L. Y., Hellier, C., Anderson, D. R., et al. 2019, *MNRAS*, 490, 2467, doi: [10.1093/mnras/stz2632](https://doi.org/10.1093/mnras/stz2632)
- Teske, J. K., Ghezzi, L., Cunha, K., et al. 2015, *ApJL*, 801, L10, doi: [10.1088/2041-8205/801/1/L10](https://doi.org/10.1088/2041-8205/801/1/L10)
- Teske, J. K., Khanal, S., & Ramírez, I. 2016, *ApJ*, 819, 19, doi: [10.3847/0004-637X/819/1/19](https://doi.org/10.3847/0004-637X/819/1/19)
- Thorngren, D. P., & Fortney, J. J. 2018, *AJ*, 155, 214, doi: [10.3847/1538-3881/aaba13](https://doi.org/10.3847/1538-3881/aaba13)
- Tittemore, W. C., & Wisdom, J. 1990, *Icarus*, 85, 394, doi: [10.1016/0019-1035\(90\)90125-S](https://doi.org/10.1016/0019-1035(90)90125-S)
- Triaud, A. H. M. J. 2018, in *Handbook of Exoplanets*, ed. H. J. Deeg & J. A. Belmonte, 2, doi: [10.1007/978-3-319-55333-7_2](https://doi.org/10.1007/978-3-319-55333-7_2)
- Trifonov, T., Brahm, R., Jordán, A., et al. 2023, *AJ*, 165, 179, doi: [10.3847/1538-3881/acba9b](https://doi.org/10.3847/1538-3881/acba9b)
- Turner, J. D., Pearson, K. A., Biddle, L. I., et al. 2016, *MNRAS*, 459, 789, doi: [10.1093/mnras/stw574](https://doi.org/10.1093/mnras/stw574)
- van der Walt, S., Colbert, S. C., & Varoquaux, G. 2011, *Computing in Science and Engineering*, 13, 22, doi: [10.1109/MCSE.2011.37](https://doi.org/10.1109/MCSE.2011.37)
- Van Eylen, V., & Albrecht, S. 2015, *ApJ*, 808, 126, doi: [10.1088/0004-637X/808/2/126](https://doi.org/10.1088/0004-637X/808/2/126)
- Virtanen, P., Gommers, R., Oliphant, T. E., et al. 2020, *Nature Methods*, 17, 261, doi: [10.1038/s41592-019-0686-2](https://doi.org/10.1038/s41592-019-0686-2)
- Vissapragada, S., Knutson, H. A., Jovanovic, N., et al. 2020, *AJ*, 159, 278, doi: [10.3847/1538-3881/ab8e34](https://doi.org/10.3847/1538-3881/ab8e34)
- Wang, L., & Dai, F. 2019, *ApJL*, 873, L1, doi: [10.3847/2041-8213/ab0653](https://doi.org/10.3847/2041-8213/ab0653)
- Wang, S., Jones, M., Shporer, A., et al. 2019, *AJ*, 157, 51, doi: [10.3847/1538-3881/aaf1b7](https://doi.org/10.3847/1538-3881/aaf1b7)
- Winn, J. N., & Fabrycky, D. C. 2015, *ARA&A*, 53, 409, doi: [10.1146/annurev-astro-082214-122246](https://doi.org/10.1146/annurev-astro-082214-122246)
- Wisdom, J. 2008, *Icarus*, 193, 637, doi: [10.1016/j.icarus.2007.09.002](https://doi.org/10.1016/j.icarus.2007.09.002)
- Wizinowich, P., Acton, D. S., Shelton, C., et al. 2000, *PASP*, 112, 315, doi: [10.1086/316543](https://doi.org/10.1086/316543)
- Wu, Y., & Murray, N. 2003, *ApJ*, 589, 605, doi: [10.1086/374598](https://doi.org/10.1086/374598)
- Yoshida, S., Vissapragada, S., Latham, D. W., et al. 2023, *AJ*, 166, 181, doi: [10.3847/1538-3881/acf858](https://doi.org/10.3847/1538-3881/acf858)
- Zahn, J. P. 1977, *A&A*, 57, 383
- Zechmeister, M., & Kürster, M. 2009, *A&A*, 496, 577, doi: [10.1051/0004-6361:200811296](https://doi.org/10.1051/0004-6361:200811296)
- Zechmeister, M., Reiners, A., Amado, P. J., et al. 2018, *A&A*, 609, A12, doi: [10.1051/0004-6361/201731483](https://doi.org/10.1051/0004-6361/201731483)
- . 2020, *SERVAL: SpEctrum Radial Velocity AnaLyser*, *Astrophysics Source Code Library*, record ascl:2006.011